Improved stability of mesoporous carbon fuel cell catalyst support through incorporation of TiO2

Bauer, Alex; Song, Chaojie; Ignaszak, Anna; Hui, Rob; Zhang, Jiujun; Chevallier, Laure; Jones, Deborah; Rozière, Jacques

Publisher's version / Version de l'éditeur:
https://doi.org/10.1016/j.electacta.2010.07.025
Electrochimica Acta, 55, 28, pp. 8365-8370, 2010-07-16

Electrochimica Acta 55 (2010) 8365–8370

Contents lists available at ScienceDirect

Electrochimica Acta

journal homepage: www.elsevier.com/locate/electacta

Improved stability of mesoporous carbon fuel cell catalyst support through incorporation of TiO_2

Alex Bauer[a,*,1], Chaojie Song[a], Anna Ignaszak[a,1], Rob Hui[a], Jiujun Zhang[a,1], Laure Chevallier[b], Deborah Jones[b,1], Jacques Rozière[b]

[a] Institute for Fuel Cell Innovation, National Research Council of Canada, 4250 Wesbrook Mall, Vancouver, B.C., Canada V6T 1W5
[b] Institut Charles Gerhardt, Agrégats, Interfaces et Matériaux pour l'Energie, UMR CNRS 5253, Université Montpellier II, 34095 Montpellier Cedex 5, France

ARTICLE INFO

Article history:
Received 4 May 2010
Received in revised form 9 July 2010
Accepted 10 July 2010
Available online 16 July 2010

Keywords:
Mesoporous carbon
Fuel cells
Platinum
Durability
Titanium dioxide

ABSTRACT

The electrochemical stability of Pt deposited on mesoporous carbon, which was either applied in its unmodified state or coated with 20 wt% TiO_2, was investigated by cyclic voltammetry in N_2 purged 0.5 M sulfuric acid. XRD analysis revealed that TiO_2 was present in the anatase phase. The mean Pt particle diameter was ~6 and ~4 nm for mesoporous carbon with and without TiO_2, respectively. Pt supported on TiO_2 modified substrates was more stable than Pt supported on conventional mesoporous carbon when subjected to 1000 cycles in the potential range from 0.05 to 1.25 V vs. RHE. This was evident from the observation that the support with TiO_2 retained ~53% of the electrochemically active surface area relative to the state observed after 100 cycles, whereas ~33% of the active area remained in the case without TiO_2. The oxygen reduction mass activity was identical for both fresh samples (i.e., 18 A g_{Pt}^{-1}). After 1000 cycles the mass activity decreased to 10 A g_{Pt}^{-1} for the case without TiO_2, whereas with TiO_2 the deactivation was minor; i.e., the mass activity after 1000 cycles was 17 A g_{Pt}^{-1}.

1. Introduction

The application of mesoporous carbon (MC) as a catalyst support material has been studied extensively due to its favorable properties for PEM fuel cell electrodes [1–10]. The high surface area allows for a fine dispersion of Pt nanoparticles, thus resulting in a large active catalyst surface. The interconnected porous structure favors the mass transport of reactants and products [9,10]. The beneficial mass transport properties are particularly relevant for direct methanol fuel cell electrodes where effective transport of methanol to the active sites and rapid removal of CO_2 gas bubbles is crucial [5,6]. Further, it was demonstrated that the performance of hydrogen PEM fuel cells improved by employing mesoporous carbon compared to using non-porous carbon or activated carbon [2,9].

A major issue concerning the catalyst support durability is carbon corrosion, which occurs at potentials that are higher than 0.9 V vs. RHE [11]. This carbon support disintegration leads to a significant loss of the active catalyst area, thereby causing a decrease of the fuel cell performance. In particular, fuel cells applied in automobiles suffer high performance losses due to carbon corrosion, as the cell potential can reach up to 1.5 V during start-up-shut-down cycles. It is therefore important to explore alternative materials that can provide improved stability compared to carbon. Several research groups investigated titanium, tungsten and zirconium oxide supports with size features in the nanometer range [12–18]. Recent results in our group showed that Pt supported on titanium dioxide nanofibers is more stable compared to conventional carbon black [18]. However, the relatively low conductivity of titania imposes a certain limitation on the performance.

TiO_2 and carbon can be combined to form nano-composite catalyst supports [19–22]. Von Kraemer et al. showed that such a modified support performed comparably to Pt/C in a PEM fuel cell [19]. Tian et al. demonstrated an improvement in durability for Pt–TiO_x/C relative to Pt/C for PEM fuel cell operation without humidification, which was explained in part by the ability of TiO_2 to retain water [22].

In this work we present the synthesis and characterization of a novel composite of mesoporous carbon and TiO_2 nanoparticles. The purpose of this approach is to achieve enhanced durability compared to conventional mesoporous carbon supports while maintaining a high conductivity and providing adequate mass transfer of the chemical species in the fuel cell catalyst layer.

* Corresponding author. Tel.: +1 604 221 3149; fax: +1 604 221 3001.
E-mail address: alexander.bauer@nrc-cnrc.gc.ca (A. Bauer).
[1] ISE member.

0013-4686/$ – see front matter © 2010 Elsevier Ltd. All rights reserved.
doi:10.1016/j.electacta.2010.07.025

2. Experimental

2.1. Mesoporous carbon synthesis

A detailed description of the mesoporous carbon fabrication was reported elsewhere [23,24]. As a first step mesoporous silica (SBA-15) was prepared by using a triblock copolymer, EO_{20}–PO_{70}–EO_{20} (Pluronic P123, BASF), and tetraethyl orthosilicate (TEOS, Aldrich) [24]. Pluronic P123 (4.0 g) was dissolved in 30 g of DI H_2O, and 120 g of 2 M HCl solution were added while stirring at 35 °C. TEOS (8.5 g) was added and the solution was stirred at 35 °C for 20 h. The mixture was then aged at 80 °C overnight without stirring. The solid was filtered, washed with water, and dried in air at 25 °C. The dried sample was calcined in air at 500 °C for 6 h.

To synthesize the mesoporous carbon, 1 g of SBA-15 was added to a solution composed of 1.25 g of sucrose and 0.14 g of H_2SO_4 in 5 g of H_2O [25]. The mixture was dried in an oven at 100 °C. Then the temperature was increased to 160 °C and maintained for 6 h. The silica sample, containing partially polymerized and carbonized sucrose, was heat-treated again in the same manner after the further addition of 0.8 g of sucrose, 0.09 g of H_2SO_4 and 5 g of H_2O. The carbonization was completed by heating to 900 °C in an inert (N_2) atmosphere. The carbon–silica composite obtained after pyrolysis was washed with 5% HF to remove the silica template. The product was filtered, washed with ethanol, and dried at 120 °C.

To incorporate the TiO_2, 0.1 g mesoporous carbon was mixed with 20 mL isopropanol, stirred for several minutes. Then 0.105 mL Ti-isopropoxide (98%, Acros) was added. The mixture was stirred overnight. Isopropanol was removed by centrifugation, and the material was further washed with acetone. The sample was air dried at $T = 80$ °C overnight. The Ti content was 20 wt%, as determined by energy dispersive X-ray spectroscopy (EDX).

2.2. Pt nanoparticle deposition

To prepare the deposition bath, 0.1 g mesoporous carbon (or TiO_2 coated MC) was mixed with 100 mL ethylene glycol and then sonicated for 10 min. The Pt precursor, 52 mg H_2PtCl_6 (Aldrich), was dissolved in 12 mL ethylene glycol and sonicated for 5 min. Further, 16 mg NaOH was dissolved in 0.4 mL ethylene glycol and sonicated for 5 min. The Pt precursor and NaOH solutions were added consecutively to the mesoporous carbon slurry while stirring. The slurry was placed in a vacuum oven at 20 °C for 1 h to facilitate the Pt precursor transport into the pores. Then the Pt deposition was carried out by heating the bath in a microwave oven, which was operated at 600 W for 90 s. The solvent was removed with a centrifuge, which was run four times for 8 min at 11,000 rpm, while replacing the liquid with fresh deionized H_2O each time. The Pt coated mesoporous carbon (or TiO_2 coated MC) was dried in an oven at 80 °C overnight.

2.3. BET area measurements

The specific surface area of the mesoporous carbon supports was measured using the Brunauer–Emmet–Teller (BET) method. The surface area analyzer was a SA3100 model built by Beckman Coulter.

2.4. XRD analysis

Powder diffraction experiments were carried out with a Bruker D8 diffractometer equipped with a graphite monochromator and a vertical goniometer, using Cu-Kα radiation.

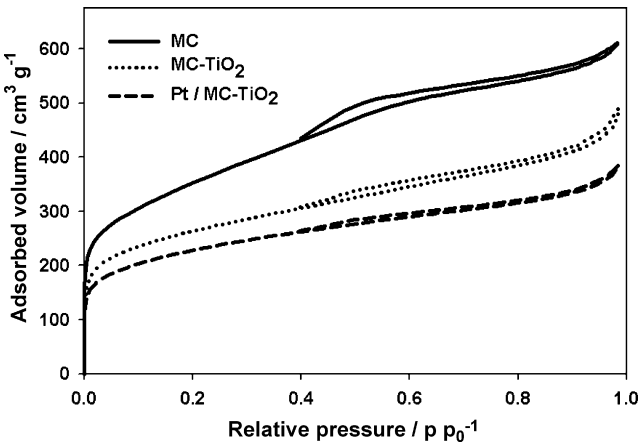

Fig. 1. N_2 adsorption–desorption isotherms for mesoporous carbon (unmodified, with TiO_2, and Pt nanoparticle coated with TiO_2).

2.5. TEM imaging

Transmission electron microscopy was carried out with a Hitachi H7600 microscope operated at 100 kV.

2.6. Electrochemical testing

All electrochemical experiments were conducted with a Solartron multistat instrument (controlled with Corrware software, Scribner Associates Inc., USA) and a three-electrode set-up in a glass cell. The working electrode was a glassy carbon rotating disk electrode (RDE) (Pine Instrument) with a geometric area of 0.196 cm^2, and a Pt wire counter electrode was employed. The reference electrode was a $Hg/HgSO_4$ type electrode, which contained a 30 wt% sulfuric acid solution (Koslow Scientific). The catalyst powder was dispersed in isopropanol by sonication for 20 min before depositing the selected Pt loading of 48 $\mu g\,cm^{-2}$ onto the electrode using a micropipette. The Pt content relative to the support material was 20 wt%. A Nafion film was cast by applying 7.1 μL of a 1:100 solution of 5 wt% Nafion in methanol onto the powder coated RDE. To clean the Pt surface each freshly prepared electrode was cycled 20 times in N_2 purged 0.5 M H_2SO_4 in the range of 0.05 to 1.2 V vs. RHE at a scan rate of 50 $mV\,s^{-1}$.

To assess the electrochemical catalyst stability, cyclic voltammetry was carried out at 100 $mV\,s^{-1}$, performing 1000 full cycles from 0.05 to 1.25 V vs. RHE. The active Pt surface observed after 100, 500 and 1000 cycles was estimated based on the H_2 adsorption charge obtained in the range from 0.05 to 0.35 V vs. RHE. A hydrogen adsorption charge of 210 $\mu C\,cm^{-2}$ was assumed for the active Pt area estimation [26].

Oxygen reduction reaction (ORR) tests were conducted using linear sweep voltammetry with O_2 saturated 0.5 M H_2SO_4. The rotation rate was 1600 rpm. The potential was decreased from 1.1 to 0.4 V vs. RHE at a scan rate of 5 $mV\,s^{-1}$. The ORR activity was determined for fresh catalysts and catalysts that were 'aged' by performing 1000 cycles as described above. All electrochemical tests were carried out at 20 °C and ambient pressure, and the current density is reported as current per geometric electrode area.

3. Results and discussion

3.1. BET

The adsorption isotherms for mesoporous carbon and mesoporous carbon coated with TiO_2 and Pt are presented in Fig. 1. As expected, the pore volume and the surface area decreased

Table 1
BET analysis for mesoporous carbon (unmodified, with TiO_2, and Pt coated with TiO_2).

	BET surface Area/$m^2\ g^{-1}$	Pore Volume/$cm^3\ g^{-1}$
MC	1255	0.94
MC–TiO_2	806	0.58
Pt/MC–TiO_2	591	0.45

Table 2
Approximate active Pt surface area [$m^2\ g_{Pt}{}^{-1}$] measured at 100, 500 and 1000 cycles. The percentage values denote the fraction of the active area that is sustained relative to the electrode surface state after 100 cycles.

Cycle #	Pt/MC	Pt/MC–TiO_2
100	24	34
500	13 54%	25 74%
1000	8 33%	18 53%

due to the addition of TiO_2 and Pt nanoparticles (see Table 1). Without Pt and TiO_2 the BET surface area was 1255 $m^2\ g^{-1}$. For comparison, Raghuveer and Manthiram reported 890 $m^2\ g^{-1}$ (pore volume = 1.05 $cm^3\ g^{-1}$) [6] for mesoporous carbon, whereas Wikander et al. obtained 1623 $m^2\ g^{-1}$ (pore volume = 1.49 $cm^3\ g^{-1}$) [1]. Joo et al. prepared several supports varying the silica precursor to carbon molar ratio [9]. The highest surface area values were 724 and 672 $m^2\ g^{-1}$ (with Pt), and the corresponding pore volumes were 2.02 and 1.7 $cm^3\ g^{-1}$, respectively. These values resulted from applying a silica to carbon ratio of 3.

3.2. XRD

The XRD patterns for mesoporous carbon with Pt catalyst are shown in Fig. 2. The measurement for the modified MC revealed that TiO_2 was present in the anatase phase, as indicated by the additional peaks at ~55° and ~64°. The Miller indices for Pt are shown in the graph. The formation of the anatase structure can be expected after the heat treatment at 900 °C in an inert atmosphere, whereas the rutile structure would form at higher temperatures in N_2 or result from heat treatment in a reducing atmosphere at similar temperatures [12]. Since the sample was treated at 900 °C we expect the TiO_2 component to be crystalline. The very high background intensity seen in the diffractograms (Fig. 2) originates from amorphous carbon. The background intensities are very similar for both Pt/MC and Pt/MC–TiO_2 samples, which suggests that no other non-crystalline phases exist within Pt/MC–TiO_2.

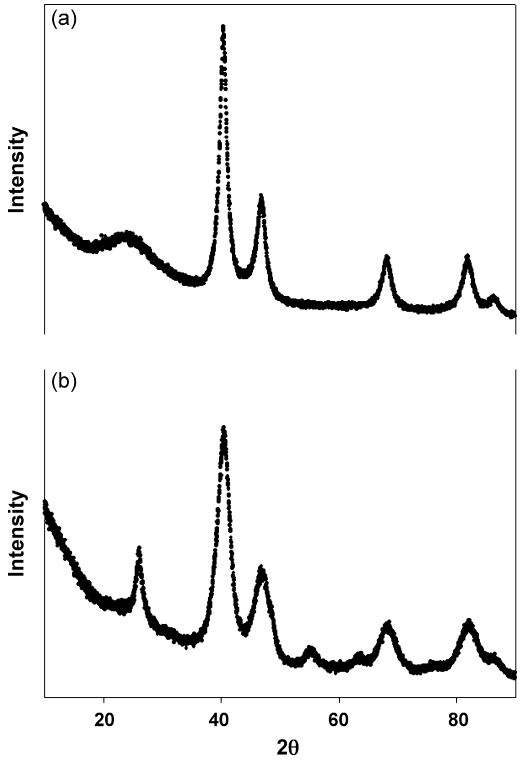

Fig. 2. Diffractograms for Pt supported on mesoporous carbon (a) and Pt supported on TiO_2 modified mesoporous carbon (b).

3.3. TEM

The Pt particle size was larger when TiO_2 was present compared to unmodified mesoporous carbon, as shown in Fig. 3. The mean Pt particle diameter increased from 3.9 to 5.9 nm. For comparison, Wikander et al. employed a water/oil microemulsion method, and observed a particle diameter of 3 nm on ordered mesoporous carbon by both TEM and STEM analysis [1]. Joo et al. reported a Pt particle size of 3.5–4 nm for deposits on mesoporous carbon obtained by reduction with formaldehyde [9]. As presented in Fig. 3, Pt is well dispersed on both the pure carbon and the TiO_2 coated carbon support, which indicates that the presence of TiO_2 does not adversely affect the homogeneity of the catalyst dispersion. Pt is probably located on both carbon and on the TiO_2 surface. The other possible location for Pt is the grain boundary between carbon and TiO_2, where Pt agglomeration may occur. This type of agglomeration would explain the increased Pt particle diameters observed for Pt on MC–TiO_2 (see histograms in Fig. 3).

3.4. Electrochemical stability assessment

As described in Section 2.6, the active Pt surface area was monitored as an indicator of the catalysts' electrochemical stability during potential cycling. The double layer charge, typically observed at ~0.4 V vs. RHE may be masked by the pronounced broad peaks at ~0.5 and ~0.6 V vs. RHE on the cathodic and anodic scans, respectively (see Fig. 4). Said peaks represent interactions with functional groups on the carbon surface [18]. The peaks obtained during the anodic sweep at higher potentials, i.e. at ~0.95 and 1.1 V vs. RHE, occurred due to the oxidation of metallic Pt to Pt^{2+} and further oxidation to Pt^{4+}, respectively. The reduction of the Pt oxides was recorded at ~0.73 V vs. RHE. Table 2 contains the approximate Pt surface areas for both supports as estimated after 100, 500 and 1000 cycles. Since the double layer charge is unknown, all reported Pt surface areas are approximate, and the reported values are likely lower than the respective true active Pt surface areas.

In general, higher surface areas were obtained with TiO_2 over the course of 1000 cycles, which is consistent with literature reports on TiO_2 modified carbon nanoparticle supports [21]. This behavior can be rationalized by assuming an improved surface wetting [27] or the formation of additional active sites at the Pt/TiO_2 interface [28]. The electrode surface state after 100 cycles was selected arbitrarily as a baseline for estimating the active area loss. The support with TiO_2 was more stable, as it allowed to sustain 53% of the active Pt area at the end of the durability test relative to the baseline. When the unmodified mesoporous carbon support was applied 67% of the catalytic surface area was lost over the course of 900 cycles. Therefore, the presence of TiO_2 improved the durability significantly. It is likely that the double layer charge is higher without TiO_2 [19], which implies that the relative surface area loss for the unmodified sample may be more pronounced (compared to the

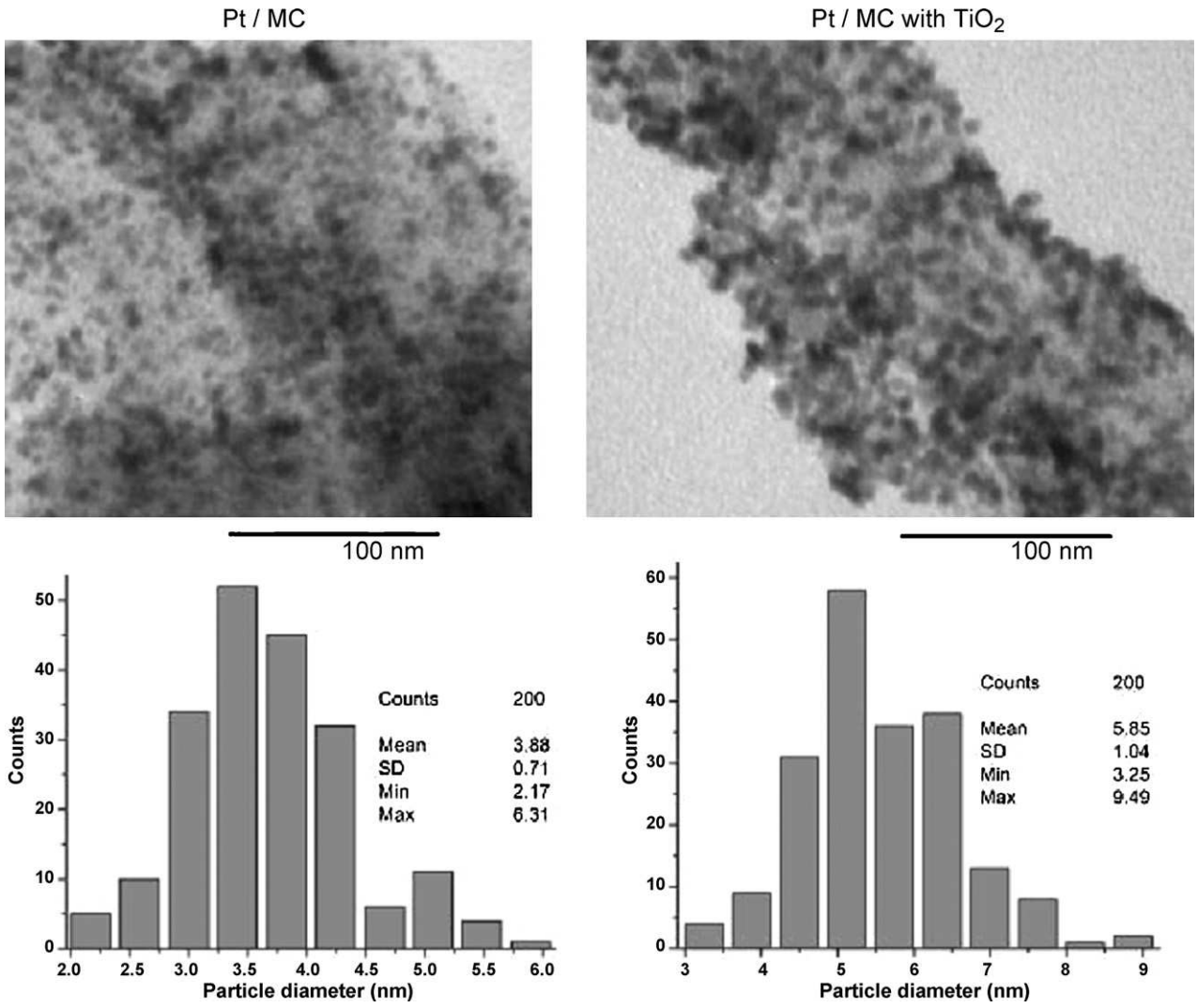

Fig. 3. TEM micrographs and particle size distributions for Pt nanoparticle deposited on mesoporous carbon and TiO_2 modified mesoporous carbon.

case with TiO_2) than the decrease indicated by the electrochemical tests. The improved stability observed for Pt/TiO_2–C can be explained by assuming that the TiO_2 component acts as an inhibitor of the catalyst degradation process, which is mostly due to catalyst detachment from the support as a result of carbon corrosion. Pt is most stable when located at the TiO_2/carbon boundary or on the TiO_2 surface. Further, parts of the carbon surface may be protected against electrochemical oxidation by the presence of overlaid titania. The Pt particles, which are located at the carbon/TiO_2 interface, stay attached to the titanium oxide during the progressive carbon degradation and therefore remain electrochemically active.

3.5. Oxygen reduction activity

The ORR measurements carried out with Pt supported on either unmodified MC or on the TiO_2–MC composite are shown in Fig. 5. In both cases there was a decrease in performance in the kinetic and mixed control regions as a result of continuous cycling. The decline was less pronounced when TiO_2 was present. The respective mass activities (measured at 0.9 V vs. RHE) are summarized in Table 3. The Tafel slopes for Pt on MC and Pt on MC–TiO_2, which were obtained in the overpotential (η) range of ~0.23–0.26 V vs. RHE (see Fig. 6), are presented in Table 3. The true kinetic current density was determined with the following equation:

$$i_k = \frac{(i \times i_L)}{(i_L - i)} \quad (1)$$

where i_L is the diffusion-limited current density and i is the measured current density [29]. The diffusion-limited current density was approximated by the current density observed at 0.4 V vs. RHE.

As shown in Table 3, the relatively high stability of the support containing titania was beneficial with respect to the ORR activity, as 94% of the Pt mass activity was retained with the aged catalyst compared to a fresh sample of the same composition (17 A g_{Pt}^{-1} vs. 18 A g_{Pt}^{-1}). Without TiO_2 a more pronounced performance drop was found as a result of the durability test: The mass activity decreased

Table 3
Oxygen reduction mass activity at 0.9 V vs. RHE and Tafel slopes for freshly prepared catalysts and catalysts that were subjected to 1000 full voltammetric scans.

		Pt/MC	Pt/MC–TiO_2
Fresh catalyst	ORR mass activity/A g_{Pt}^{-1}	18	18
	Tafel slope/mV dec^{-1}	113	107
'Aged' catalyst	ORR mass activity/A g_{Pt}^{-1}	10	17
	Tafel slope/mV dec^{-1}	129	100

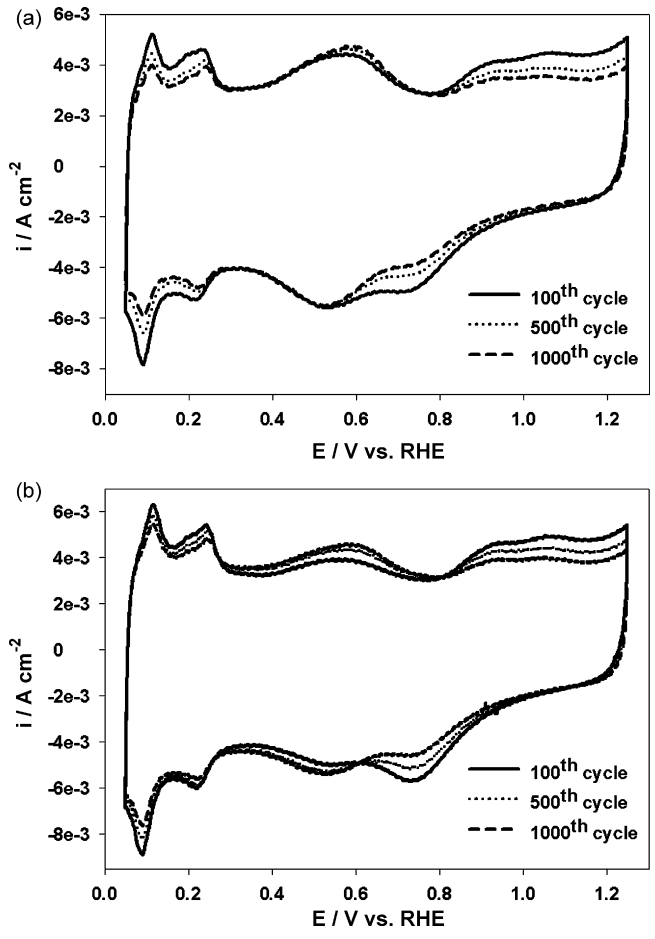

Fig. 4. Voltammetric stability test. Pt supported on mesoporous carbon (a) and TiO_2 modified mesoporous carbon (b). Conditions: 0.5 M H_2SO_4, 100 mV s^{-1}, 20 °C.

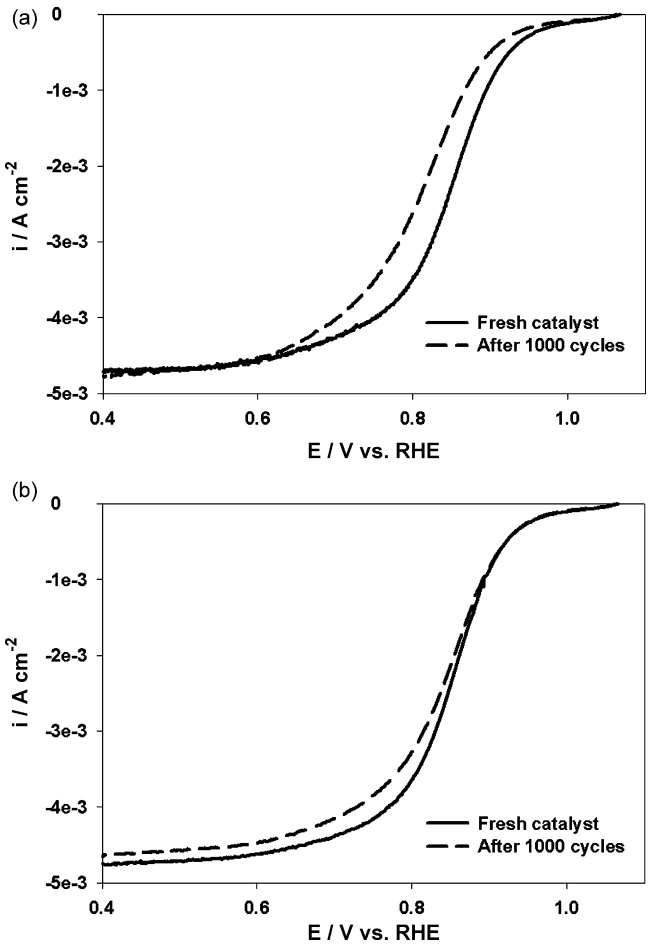

Fig. 5. Oxygen reduction activity tests with unmodified (a) and TiO_2 modified mesoporous carbon (b). Comparison of fresh and aged catalysts. Conditions: 0.5 M H_2SO_4, 5 mV s^{-1}, 1600 rpm, 20 °C.

from 18 to 10 A g_{Pt}^{-1}. For comparison, a mass activity of 43 A g_{Pt}^{-1} was reported at ~0.9 V vs. RHE for an E-tek type commercial catalyst (i.e., Pt supported on Vulcan XC-72 carbon particles), whereas Pt on supported porous carbon with a surface area of ~700 m^2 g^{-1} yielded a mass activity of ~3 A g_{Pt}^{-1} [30]. Carbon is the crucial component within the TiO_2 modified support regarding the electron transfer due to its significantly higher conductivity compared to TiO_2. Since rutile has only a slightly lower band gap relative to anatase one can expect that no activity enhancement would result from replacing anatase with rutile [31–33]. However, doping the titania with e.g., Nb would enhance the conductivity (and stability) and may therefore further improve the ORR activity of Pt/TiO_2–C [18].

The higher activity of Pt supported on titania-modified carbon, which was observed after extended cycling, is a result of the catalyst stability provided by TiO_2, which mainly affects Pt located either on the TiO_2 surface or on the grain boundary between carbon and TiO_2, as discussed in Section 3.4.

The Tafel slope for both fresh catalysts (Pt/MC and Pt/MC–TiO_2) is similar, indicating that the presence of TiO_2 did not change the ORR mechanism [34]. After performing the 1000 cycle durability experiments the Tafel slope increased for the case without TiO_2 whereas a slight decrease occurred with TiO_2. The increase in Tafel slope for Pt/MC indicates that the transfer coefficient of the ORR decreased, meaning that the ORR kinetics became more sluggish after potential cycling. While for the TiO_2 modified MC, the slight increase in Tafel slope indicates a subtle transfer coefficient increase, i.e., faster reaction kinetics. This is unusual, since typically catalyst degradation occurs after extended potential cycling, leading to slower reaction kinetics. The faster kinetics might be due to an enhanced interaction between Pt and TiO_2. Due to potential cycling, there might be morphology and/or phase changes for both Pt and TiO_2, enhancing their interaction.

The Tafel slopes are high compared to the theoretical value (60 mV dec^{-1} [35]) and selected experimental data. For example, measurements conducted by Kucernak et al. yielded a Tafel slope of 58 mV dec^{-1} for mesoporous Pt attached to a microelectrode [36]. Guilminot et al. obtained 70 mV dec^{-1} for a commercial E-tek catalyst and ~70–80 mV dec^{-1} for porous carbon supported Pt [30]. We propose that there likely are intrinsic mass transport limitations due the porous nature and thickness of the support. Banham et al. demonstrated that an increase in pore length (i.e., larger catalyst layer thickness) causes an increase in the Tafel slope [34]. The Tafel slopes in the high current density regime were in the range of 170–200 mV dec^{-1} (not shown). The high values (theoretical value: 120 mV dec^{-1} [35]) are most likely due to the same effects that are described above. The shift in the Tafel slope due to the transition from the low to the high current density regime is commonly observed, and can be explained by different effects: (i) A change of the charge-transfer coefficient [37,38], (ii) different reactant adsorption mechanisms (Temkin vs. Langmuir mechanism for low and high current regimes, respectively) [35,39], (iii) a change in surface coverage with oxygen-containing species [40], and (iv) further porosity related diffusion effects [41,42].

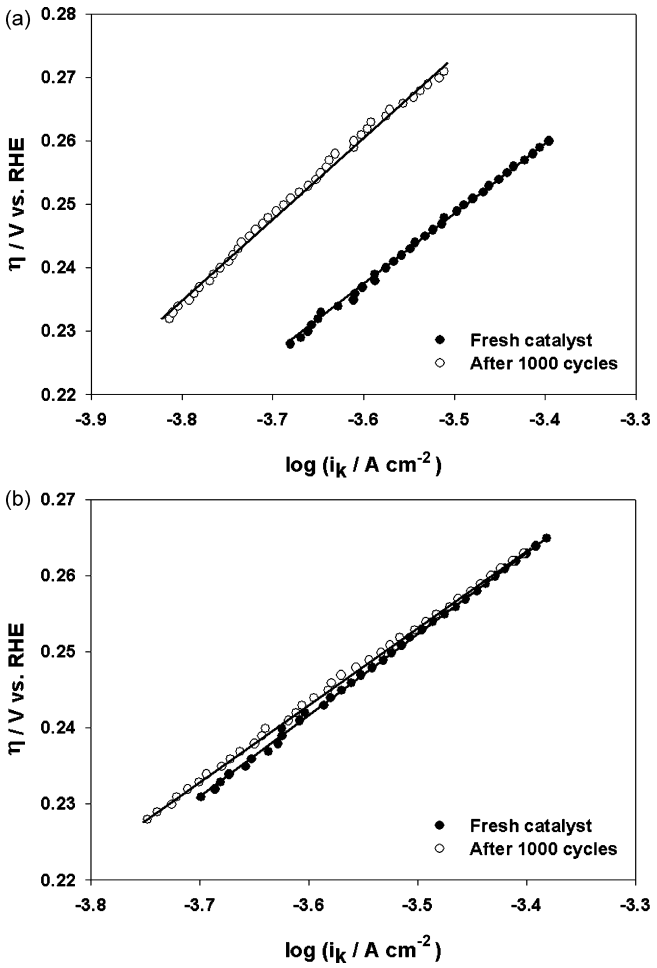

Fig. 6. Mass transfer corrected Tafel plots for Pt supported on unmodified (a) and TiO_2 modified (b) mesoporous carbon. Comparison of fresh and aged catalysts.

4. Summary and conclusions

TiO_2 modified and conventional mesoporous carbon supports were synthesized and characterized by BET, XRD, TEM and voltammetry. The incorporation of TiO_2 into mesoporous carbon catalyst support materials significantly improved the durability of the Pt catalyst support composite, as was demonstrated by cyclic voltammetry. The TiO_2 induced stability enhancement effect was also observed when the ORR activities of fresh and aged catalysts were compared. A minor mass activity deterioration of 1 A g_{Pt}^{-1} was measured for TiO_2 coated MC. By contrast, the ORR activity decreased by 8 A g_{Pt}^{-1} for conventional mesoporous carbon, which corresponds to a deterioration of ~44%. In summary, this study illustrates the potential benefits of incorporating TiO_2 into mesoporous carbon. It may be useful to expand the investigation and explore the impact of further varying the Ti concentration on the porous structure and the resulting ORR performance and the catalyst stability.

Acknowledgement

Financial support under the NRC-CNRS Cooperation Agreement "Nano-composite Catalysts for High Temperature PEM Fuel Cells" is acknowledged with thanks.

References

[1] K. Wikander, A.B. Hungria, P.A. Midgley, A.E.C. Palmqvist, K. Holmberg, J.M. Thomas, J. Colloid Interface Sci. 305 (2008) 204.
[2] J.B. Joo, P. Kim, W. Kim, J. Yi, J. Electroceram. 17 (2006) 713.
[3] G.S. Chai, I.S. Shin, J.S. Yu, Adv. Mater. 16 (22) (2004) 2057.
[4] F. Su, J. Zeng, Y. Yu, L. Lv, J.Y. Lee, X.S. Zhao, Carbon 43 (2005) 2366.
[5] V. Raghuveer, A. Manthiram, J. Electrochem. Soc. 152 (8) (2005) A1504.
[6] V. Raghuveer, A. Manthiram, Electrochem. Solid-State Lett. 7 (10) (2004) A336.
[7] J. Ding, K.-Y. Chan, J. Ren, F.-S. Xiao, Electrochim. Acta 50 (2005) 3131.
[8] H. Chang, S.H. Joo, C. Pak, J. Mater. Chem. 17 (2007) 3078.
[9] J.B. Joo, P. Kim, W. Kim, J. Kim, J. Yi, Catal. Today 111 (2006) 171.
[10] H. Yamada, T. Haira, I. Moriguchi, T. Kudo, J. Power Sources 164 (2007) 538.
[11] L. Roen, C. Paik, T. Jarvi, Electrochem. Solid-State Lett. 7 (2004) A19.
[12] H. Chhina, S. Campbell, O. Kesler, J. Electrochem. Soc. 156 (2009) B1232.
[13] H. Chhina, D. Susac, S. Campbell, O. Kesler, Electrochem. Solid-State Lett. 12 (2009) B97.
[14] E. Antolini, E.R. Gonzalez, Solid-State Ionics 180 (2009) 746.
[15] N. Rajalakshmi, N. Lakshmi, K.S. Dhathathreyan, Int. J. Hydrogen Energy 33 (2008) 7521.
[16] E. Forno, E. Lee, D. Campbell, Y. Xia, Nano Lett. 8 (2008) 668.
[17] S.-Y. Huang, P. Ganesan, S. Park, B.N. Popov, J. Am. Chem. Soc. 131 (2009) 13898.
[18] A. Bauer, K. Lee, C. Song, Y. Xie, J. Zhang, R. Hui, J. Power Sources 195 (10) (2010) 3105.
[19] S. von Kraemer, K. Wikander, G. Lindbergh, A. Lundblad, A.E.C. Palmqvist, J. Power Sources 180 (2008) 185.
[20] K. Wikander, H. Ekström, A.E.C. Palmqvist, A. Lundblad, K. Holmberg, G. Lindbergh, Fuel Cells 6 (2006) 21.
[21] L. Xiong, A. Manthiram, Electrochim. Acta 49 (2004) 4163.
[22] J. Tian, G. Sun, M. Cai, Q. Mao, Q. Xin, J. Echem. Soc. 155 (2) (2008) B187.
[23] J.H. Nam, Y.-Y. Jang, Y.-U. Kwon, J.-D. Nam, Electrochem. Commun. 6 (2004) 737.
[24] D. Zhao, Q. Huo, J. Feng, B.F. Chmelka, G.D. Stucky, J. Am. Chem. Soc. 120 (1998) 6024.
[25] S. Jun, S.H. Joo, R. Ryoo, M. Kruk, M. Jaroniec, Z. Liu, T. Ohsuna, O. Terasaki, J. Am. Chem. Soc. 122 (2000) 10712.
[26] F.C. Nart, W. Vielstich, Handbook of Fuel Cells: Fundamentals, Technology, and Applications, vol. 2, John Wiley and Sons Inc., Hoboken, NJ, 2003, p. 302.
[27] G. Tamizhmani, G.A. Capuano, J. Electrochem. Soc. 141 (1994) 968.
[28] J. Shim, C.-R. Lee, H.-K. Lee, J.-S. Lee, E.J. Cairns, J. Power Sources 102 (2001) 172.
[29] H.A. Gasteiger, S.S. Kocha, B. Sompalli, F.T. Wagner, Appl. Catal. B: Environ. 56 (1–2) (2005) 9.
[30] E. Guilminot, R. Gavillon, M. Chatenet, S. Berthon-Fabry, A. Rigacci, T. Budtova, J. Power Sources 185 (2008) 717.
[31] K.-W. Park, K.-S. Seol, Electrochem. Commun. 9 (2007) 2256.
[32] M. Grätzel, Nature 414 (2001) 338.
[33] A. Fujishima, K. Honda, Nature 238 (1972) 37.
[34] O.A. Baturina, Y. Garsany, T.J. Zega, R.M. Stroud, T. Schull, K.E. Swider-Lyons, J. Electrochem. Soc. 155 (2008) B1314.
[35] D.W. Banham, J.N. Soderberg, V.I. Birss, J. Phys. Chem. C 113 (2009) 10103.
[36] A. Kucernak, J. Jiang, Chem. Eng. J. 93 (2003) 81.
[37] N.M. Markovic, P.N. Ross, Surf. Sci. Rep. 45 (2002) 117.
[38] M. Van Brussel, G. Kokkinidis, A. Hubin, C. Buess-Herman, Electrochim. Acta 48 (2003) 3909.
[39] T.J. Schmidt, U.A. Paulus, H.A. Gasteiger, R.J. Behm, J. Electroanal. Chem. 508 (2001) 41.
[40] N.M. Markovic, R.R. Adzic, B.D. Cahan, E.B. Yeager, J. Electroanal. Chem. 377 (1994) 249.
[41] J. Perez, A.A. Tanaka, E.R. Gonzales, E.A. Ticianelli, J. Electrochem. Soc. 141 (1994) 431.
[42] J. Perez, E.R. Gonzales, E.A. Ticianelli, Electrochim. Acta 44 (1998) 1329.